

Mechanical properties of nanocrystalline and epitaxial TiN films on (100) silicon

H. Wang, A. Sharma, and A. Kvit

Department of Materials Science and Engineering, North Carolina State University, Raleigh, North Carolina 27695-7916

Q. Wei

North Carolina A&T State University, Greensboro, North Carolina 27411

X. Zhang, C.C. Koch, and J. Narayan

Department of Materials Science and Engineering, North Carolina State University, Raleigh, North Carolina 27695-7916

(Received 26 February 2001; accepted to July 2001)

We investigated mechanical properties of TiN as a function of microstructure varying from nanocrystalline to single crystal TiN films deposited on (100) silicon substrates. By varying the substrate temperature from 25 to 700 °C during pulsed laser deposition, the microstructure of TiN films changed from nanocrystalline (having a uniform grain size of 8 nm) to a single crystal epitaxial film on the silicon (100) substrate. The microstructure and epitaxial nature of these films were investigated using x-ray diffraction and high-resolution transmission electron microscopy. Hardness measurements were made using nanoindentation techniques. The nanocrystalline TiN contained numerous triple junctions without any presence of amorphous regions. The width of the grain boundary remained constant at less than 1 nm as a function of boundary angle. Similarly the grain boundary structure did not change with grain size. The hardness of TiN films decreased with decreasing grain size. This behavior was modeled recently involving grain boundary sliding, which is particularly relevant in the case of hard materials such as TiN.

I. INTRODUCTION

High-temperature ceramics constitute a very useful class of materials due to their high melting point, strength, and stability at elevated temperatures. For example, TiN films are successfully applied as wear-protection coatings for tools and mechanical components^{1–5} decoration coatings,^{6–8} electrical contacts, and diffusion barriers in electronic devices,^{9,10} because of their excellent corrosion and erosion resistance, high hardness, high thermal stability and desirable optical, and electrical properties. However, there are disadvantages associated with these materials in terms of poor toughness and ductility that severely limit their applications. Poor toughness and ductility result from the lack of dislocations and mobility. To alleviate some of these problems, reduction of grain size can enhance grain-boundary sliding and grain boundary diffusion related creep phenomena. In the nanoscale regime, we envisage that grain-boundary sliding and creep phenomena may dominate and control the mechanical properties of TiN nanocrystalline films.

Polycrystalline TiN films have been formed by a variety of techniques such as ion beam assisted deposition,¹¹ plasma immersion ion implantation,¹² reactive

magnetron deposition,¹³ laser assisted chemical vapor deposition,¹⁴ metalorganic chemical vapor deposition,¹⁵ and pulsed laser deposition (PLD).¹⁶ Compared to other techniques, PLD offers a unique advantage in terms of low-temperature deposition, where the grain size can be varied from nano (nm), to micro (μm), to epitaxial single crystal simply by changing the substrate temperature from 25 to 700 °C. This advantage is derived primarily from the fact that the average energy of laser ablated species is about 200–1000 kT compared to kT in equilibrium techniques. As a result, this excess kinetic energy is utilized in the crystallization process on the substrate. In this paper, we have investigated mechanical properties of TiN films deposited on a (100) silicon substrate where grain size varied from the nanocrystalline regime to a single crystal. Another characteristic of the microstructure produced by this technique was the dislocation density within the grains was quite high $>10^{11} \text{ cm}^{-2}$. In most materials, hardness increases with decreasing grain size. In metallic materials, which exhibit plastic deformation, hardness that scales with yield stress increases with decreasing grain size (d) according to the Hall-Petch relationship^{17,18} ($H = H_0 + kd^{-1/2}$) where H_0 is the lattice frictional stress and k is a constant. Brittle ceramics, which fail in the elastic regime, also exhibit increasing

hardness and fracture strength with decreasing grain size.¹⁹ In the larger grain size regime a $d^{-1/2}$ dependence is observed, which is believed to be due to the scaling of “Griffith Crack” flaws with grain size (so-called Orowan branch). As the grain size decreases, the hardness/strength becomes essentially independent of grain size as flaws larger than the grain size or surface flaws become controlling (so-called Petch branch). These explanations for the grain size dependence of hardness in brittle ceramics are still controversial.¹⁹ At the nanoscale grain sizes (<30 nm), in ductile metals, dislocation based deformation apparently ceases and deformation associated with the grain boundaries (grain boundary sliding or creep) is believed to occur. In some cases a softening (“inverse Hall-Petch effect”) with decreasing grain size is observed.^{20,21} Many of the experimental observations for the inverse Hall-Petch effect are now believed to be due to artifacts, but several experimental examples of artifact free materials have been noted.²² The critical grain size where softening begins has been found to be 7 nm for Cu, which is also consistent with computer simulation results.^{21,23} For Zn, this critical grain size is found to be 11 nm.²⁴ In a hard, brittle material such as TiN, the critical grain size for softening due to grain boundary deformation may be larger than the above values for metals since dislocation activity is limited even in larger grain samples. Therefore, the primary focus of this investigation is the study of the dependence of hardness on the grain size in a hard, brittle material, specifically TiN.

II. EXPERIMENTAL

Laser physical vapor deposition of TiN was carried out using a Pulsed KrF excimer laser ($\lambda = 248$ nm, $t_p = 25$ ns, repetition rate 10 Hz) described elsewhere.^{10,16} The target was hot-pressed stoichiometric TiN obtained from CERAC Inc., Milwaukee, WI. The laser beam was focused to obtain an energy density of approximately 10 Jcm^{-2} at 45° angle of incidence. The target was held parallel to (100) silicon substrate and 4.5 cm away from it, which was cleaned ultrasonically 5 min in acetone and 1 min in methanol, followed by 1 min dip in 20% HF. All TiN films were deposited at a base pressure of about 1×10^{-7} torr with a turbomolecular pump. The laser deposition at 10 Hz repetition rate resulted in approximately 180-nm to 500-nm-thick TiN film. By varying the substrate temperature from room temperature to 700°C , the structure of TiN films changed from polycrystalline to single crystal film while keeping the film thickness constant. All the films were characterized by x-ray diffraction (XRD), high-resolution transmission electron microscopy (HRTEM) (cross-section, plan-view). Selected-area-diffraction patterns, from large specimen areas, were used to investigate

the textured and epitaxial growth of TiN films. The hardness H and elastic modulus E of the films were measured by using a nanoindenter method.

III. RESULTS AND DISCUSSION

Figure 1 shows a bright-field (BF) plan-view transmission electron microscopy (TEM) micrograph of the nanocrystalline TiN film deposited at 25°C . The average grain size was determined to be about 8 nm. The selected-area diffraction (SAD) pattern from $\langle 110 \rangle$ cross-section specimens covering both of the film and the substrate, is shown in Fig. 2(a). Figure 2(b) is the plan-view selected area diffraction pattern for the film deposited at 25°C . It is interesting to note that these nanocrystallites with average size 8 nm exhibit $\langle 100 \rangle$ texturing and the texturing becomes quite prominent as the substrate deposition temperature increases to 200°C shown in cross-section selected-area-diffraction pattern Fig. 2(c). Finally the film becomes epitaxial single crystal above 600°C , as revealed by SAD pattern from the $\langle 110 \rangle$ cross-section Fig. 3(a). The selected-area-diffraction pattern in Fig. 3 was obtained using a large aperture that covered over $2 \mu\text{m}$ diameter area of the film with some silicon substrate contribution. The pattern in Fig. 3(a) contains both silicon and TiN diffraction spots corresponding to $\langle 011 \rangle$ orientation. The simulated pattern in Fig. 3(b) clearly shows that TiN has grown epitaxially cube-on-cube via domain epitaxy where four lattice constants of TiN match with three of silicon. The SAD patterns from other areas were identical to this one, indicating TiN has grown epitaxially on silicon over a large area.

We have investigated the nature of the grain boundary as a function of deposition temperature from 25 to 500°C . Figure 4(a) and 4(b) show low-resolution (bright

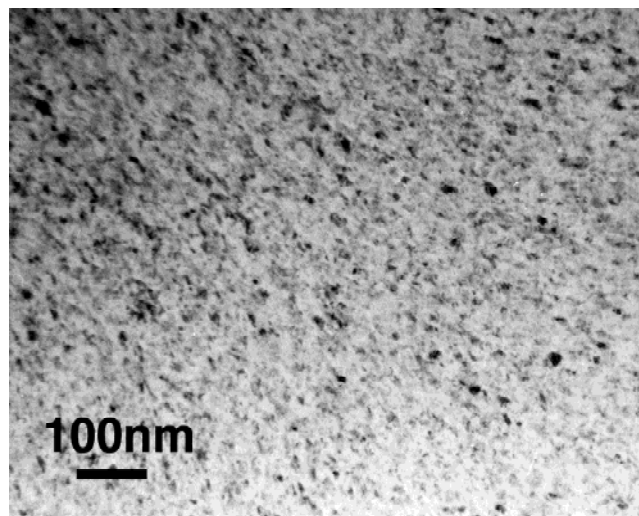


FIG. 1. BF plan-view TEM showing nanocrystalline TiN with average grain size approximately 8 nm (Substrate temperature of deposition, $T_s = 25^\circ\text{C}$).

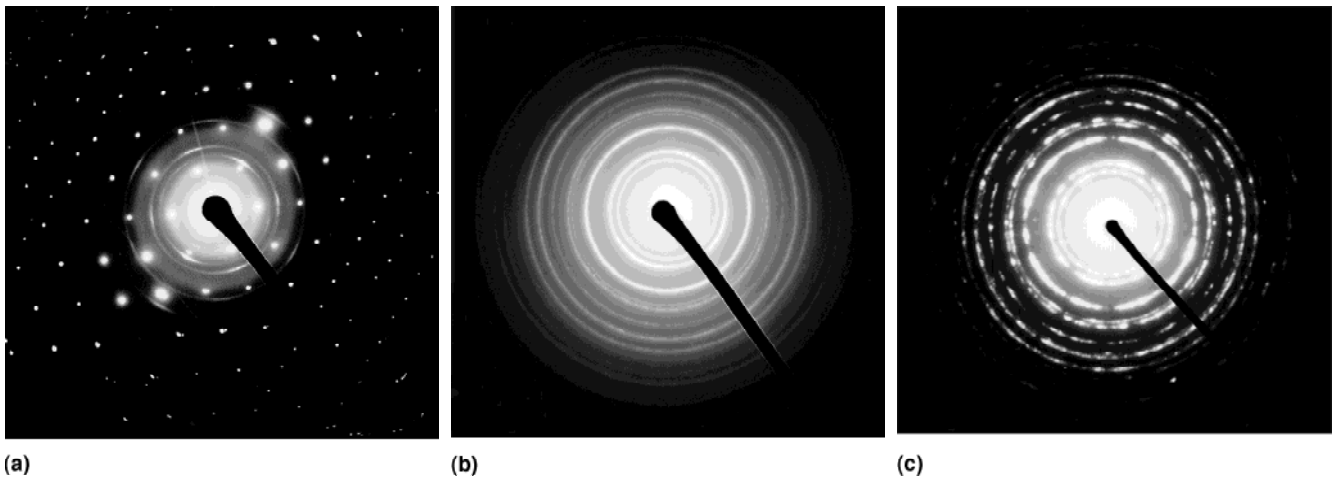


FIG. 2. Selected-area-diffraction patterns of TiN films on Si(100) deposited at different temperatures (a) $T_S = 25\text{ }^\circ\text{C}$, cross-section; (b) $T_S = 25\text{ }^\circ\text{C}$, plan-view; and (c) $T_S = 200\text{ }^\circ\text{C}$, plan-view.

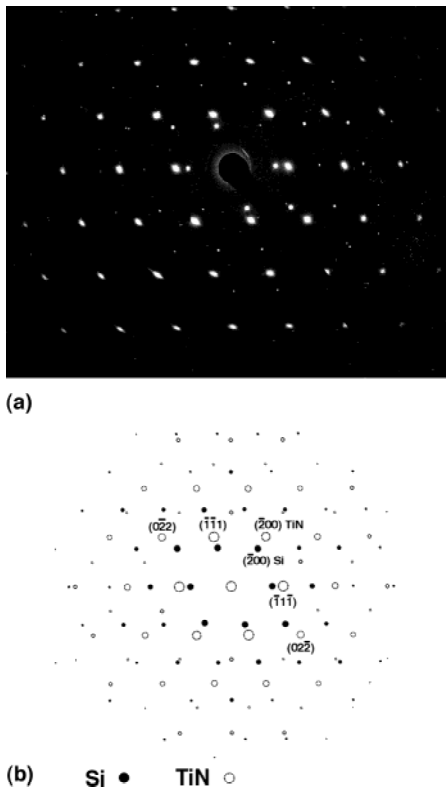


FIG. 3. (a) Selected-area-diffraction pattern of TiN film on Si(100) deposited at $700\text{ }^\circ\text{C}$, cross-section, TiN $\langle 110 \rangle$ //Si $\langle 110 \rangle$; (b) simulated diffraction pattern showing cube-on-cube TiN epitaxial growth on Si(100).

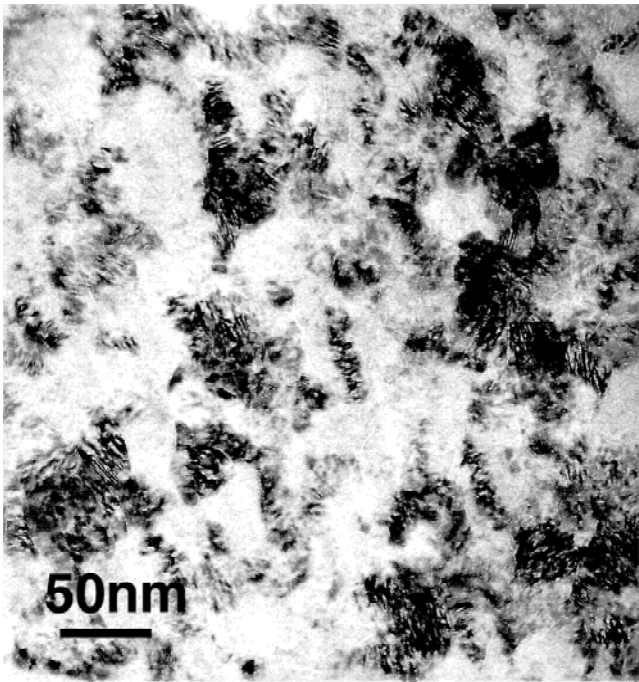
field) and high-resolution plan-view TEM micrographs, respectively, from the film deposited at $200\text{ }^\circ\text{C}$. The average grain size in the film deposited at $200\text{ }^\circ\text{C}$ was found to be 35 nm . From the low-resolution micrograph, the presence of high density of dislocations within the grains is clearly resolved. The high-resolution micrograph shows a triple boundary junction. The width of the

boundaries was determined to be less than 1 nm , similar to conventional large-grain size materials, and this width remained constant with grain size. None of these boundaries showed the presence of amorphous regions.

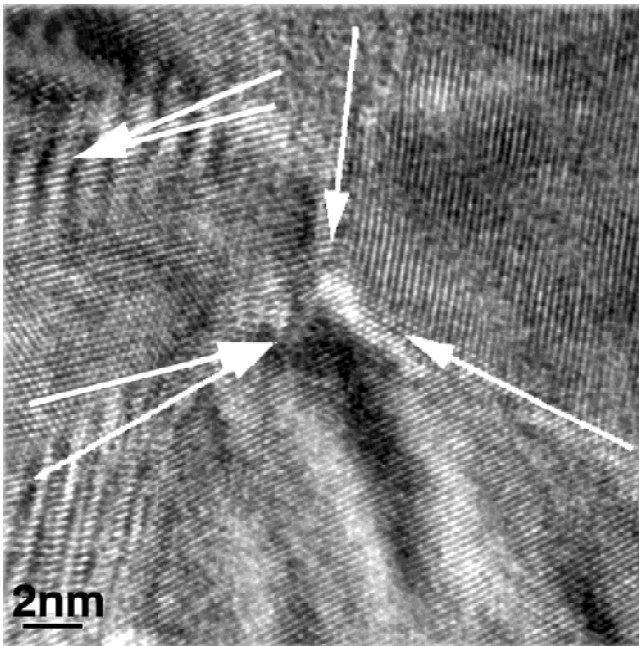
Several authors²⁵ have reported the variations in interplanar spacing as a function of nanocrystalline grain size using HRTEM imaging. These results were interpreted to result from relaxation of the nanocrystallites, where spacing increases with decreasing grain size. To investigate this effect, we have utilized diffraction information to extract planar spacings, which are more reliable than images due to deformation and information transfer. With this background, we determined the lattice constant of TiN from specimens with the 8 nm grain size to the single crystal phase. From the SAD pattern using the silicon substrate as a standard, the lattice constant was found to remain constant within the accuracy of our measurements at $0.4244 \pm 0.0016\text{ nm}$. These results were found to be in good agreement with XRD results shown in Fig. 5.

HRTEM of TiN/Si interface for the specimen deposited at $700\text{ }^\circ\text{C}$ with $\langle 110 \rangle$ normal to the specimen is shown in Fig. 6. Both sets of $\{111\}$ planes in the Si and TiN and the epitaxial growth relation are clearly visible. The $\{111\}$ planes in silicon with 0.3144 nm spacing are aligned with $\{111\}$ TiN planes with 0.2449 nm spacing. The micrograph shows the epitaxial growth of TiN even in the presence of an interfacial layer of oxide.

Figure 5 shows a XRD of TiN film ($T_S = 700\text{ }^\circ\text{C}$) on the (100) silicon substrate. The pattern contains (200) and (400) TiN along with (400) silicon diffraction showing that TiN film is textured with $[100]$ of TiN aligned with $[100]$ of silicon. The measured d -space for TiN (200) is 0.2128 nm . The lattice constant of TiN film was determined to be 0.4256 nm , which is very near to the value calculated by the selected-area-diffraction pattern result mentioned above.



(a)



(b)

FIG. 4. (a) BF plan-view micrograph and (b) high-resolution image (showing triple junction in grain boundaries) in a crystalline film deposited at $T_s = 200^\circ\text{C}$.

The variation of hardness of nanocrystalline TiN films on Si (100) with grain size is shown in Fig. 7(a). By decreasing the deposition temperature, the average grain size of TiN nanocrystalline films decreases from 55 nm ($T_s = 600^\circ\text{C}$) to 8 nm ($T_s = 25^\circ\text{C}$), and the hardness decreased from 31.9 to 25.5 GPa, which clearly shows an apparent softening. The apparent softening seems to

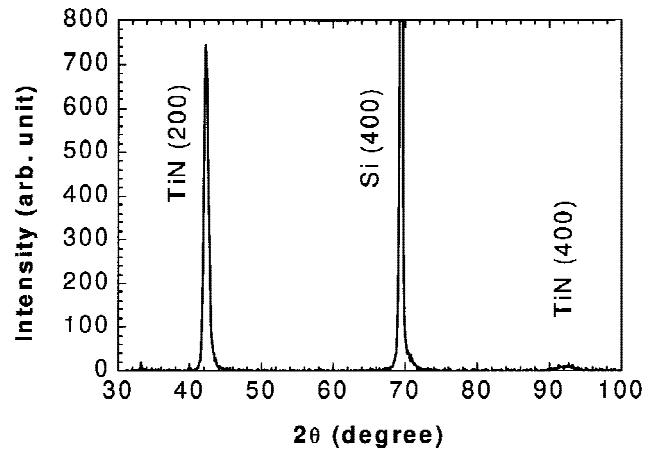


FIG. 5. XRD pattern showing (100) peaks from TiN film ($T_s = 700^\circ\text{C}$) and Si(100) substrate.

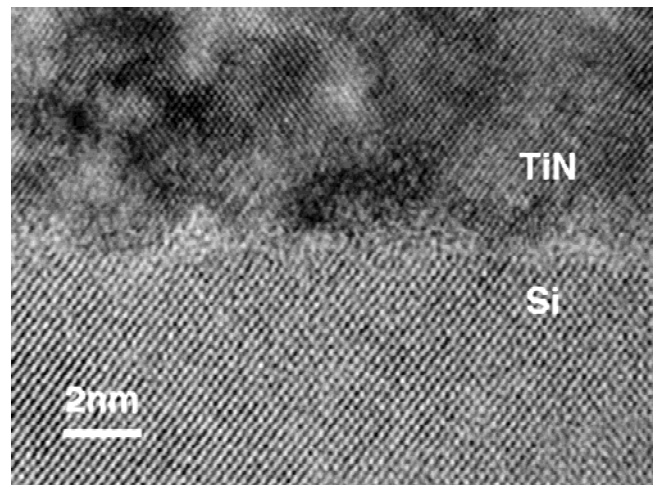


FIG. 6. High resolution $\langle 110 \rangle$ cross-section image of epitaxial TiN ($T_s = 700^\circ\text{C}$) on Si(100).

have two regions, a rapid decrease up to grain size of 35 nm, followed by a slow decrease in hardness from 35 to 8 nm. This softening behavior represents an example of the inverse Hall-Petch effect observed in some nanocrystalline metals, but in this case at much larger grain sizes. While TiN is a hard brittle material, the plastic deformation under the nanoindenter is likely to involve grain boundary deformation, as opposed to conventional dislocation motion. For TiN, the critical size for softening is estimated to be more than 55 nm, which is much larger than Zn (11 nm) and Cu (7 nm), due to the lack of dislocation activity in a hard material like TiN. The decrease in hardness followed d^n behavior where n was found to be -0.4 and -1.2 shown in Fig. 7(b). The typical softening process of nanocrystalline TiN films can be reasoned as the low angle grain boundary sliding and triple junction activity, which are proved by the high resolution plan-view micrograph shown in Fig. 4(b). This behavior has been modeled by Conrad and Narayan²⁰ and Narayan.²¹ When the grain

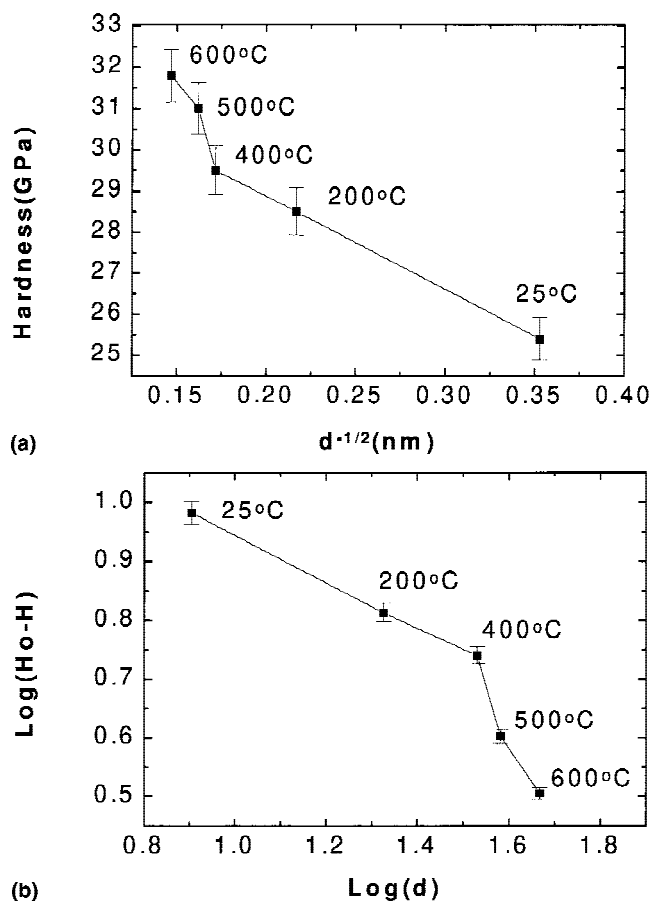


FIG. 7. (a) Hardness vs grain-size plot of nanocrystalline TiN films deposited at different temperatures (from room temperature to 600 °C); (b) log(hardness) vs. log(grain size) plot of nanocrystalline TiN films.

size decreased, the ratio of atoms in the grain boundary to those in the grains became larger and the diffusion involving grain boundary sliding became easier. Additionally, relaxation of low angle grain boundaries and triple junctions also assume an important role in the softening process. It should be noted that dislocation density within TiN grains is quite high even at large-grain sizes, which is related to processing characteristics. Thus, during subsequent deformation it may not be possible to increase the number density of dislocations in the intragrain regions. We envisage intergrain deformation via grain boundary sliding to be a primary source for deformation/softening. The Coble creep involving diffusion along the grain boundaries is not considered to be a primary source of ductility or softening for two reasons: first, TiN is a well-known diffusion barrier implying low diffusivity (high activation energy for diffusion) in TiN. The activation energy for diffusion along grain boundaries in ceramic materials is close to half of the bulk value.²⁶ Thus, at room temperature significant mass transport along grain boundaries, which seems to have normal dislocation structure, is not possible. Second, the grain

boundary sliding, which involves dislocation motion along the boundaries, can lead to a mass transport at much lower temperatures. The dislocation motion (glide) involves cooperative kink and jog motion along the dislocations where mass transport via atomic diffusion process is slow primarily due to the high activation energies involved. Because the hardness is related to the resistance of deformation, any hindrance to dislocation motion can lead to enhanced hardness. The dislocation content/density in large grains, single crystal films, or bulk materials, may account for some variations in hardness values. Thus, processing methods particularly in TiN lead to slightly different hardness values.²⁷ The hardness for TiN single-crystal film deposited at 700 °C was found to be 29 GPa, which is slightly smaller than the value for the textured film deposited at 600 °C (31.9 GPa). We envisage this drop to be related to the decrease in overall dislocation density in these single-crystal films. Similarly, higher hardness of superlattices (TiN/VN and TiN/VNbN) in the range of 31–41 GPa is envisaged to be related to the interfacial resistance to dislocation motion.²⁸

IV. SUMMARY

Using pulsed laser deposition, the grain size of TiN was varied from 8 nm to an epitaxial single crystal by changing the substrate temperature from 25 to 700 °C. The boundary angles are noncoincidence site lattice (CSL) indicating the nonequilibrium nature of the dislocation arrangement. However, the grain boundary width remained the same at less than 1 nm. The hardness of the TiN film was found to decrease with grain size of the crystal film. The decrease in hardness followed d^n behavior where n was found to be -0.4 and -1.2 . This decrease in hardness with decreasing grain size is interpreted due to intergrain deformation or grain boundary sliding as proposed by Narayan and Conrad.^{20,21}

ACKNOWLEDGMENTS

The research was supported by the National Science Foundation. C.C.K. and J.N. would also like to acknowledge additional support through Grant No. DMR-9871980 (Dr. Bruce MacDonald as Program Officer).

REFERENCES

1. R. Buhl, H.K. Pulker, and E. Moll, *Thin Solid Films* **80**, 265 (1981).
2. K. Nakamura, K. Inagawa, K. Tsuruoka, and S. Komiya, *Thin Solid Films* **40**, 155 (1977).
3. R.L. Hatscheck, *Am. Mach. Special Report No. 752*, March (1983), p. 129.
4. A. Shenhar, I. Gotman, S. Radin, P. Ducheyne, and E.Y. Gutmanas, *Surf. Coat. Technol.* **126**, 210 (2000).
5. J. Musil, *Surf. Coat. Technol.* **125**, 341 (2000).

6. B. Zega, M. Kormann, and J. Amiguet, *Thin Solid Films* **54**, 577 (1977).
7. P. Roquiny, G. Mathot, G. Tewagne, F. Bodart, and P. van den Brande, *Nuclear Instruments & Methods in Physics Research, Section B* **161–163**, 600 (2000).
8. N. Vershinin, K. Filomov, B. Straumal, W. Gust, I. Wiener, E. Rabkin, and A. Kazakevich, *Surf. Coat. Technol.* **125**, 229 (2000).
9. M. Wittmer, B. Studer, and H. Melchiar, *J. Appl. Phys.* **52**, 5722 (1981).
10. J. Narayan, P. Tiwari, J. Singh, R. Chowdhury, and T. Zheleva, *Appl. Phys. Lett.* **61**, 1290 (1992); J. Narayan, U.S. Patent No. 5 406 123 (11 April 1995).
11. J.W. Gerlach, T. Kraus, S. Sienz, M. Moske, M. Zeitler, and B. Rauschenbach, *Surf. Coat. Technol.* **103–104**, 281 (1998).
12. K. Volz, W. Ensinger, B. Stritzker, and B. Rauschenbach, *Surf. Coat. Technol.* **103–104**, 251 (1998).
13. P. Patsalas, C. Chariridis, S. Logothetidis, C.A. Dimitridis, and O. Valassiades, *J. Appl. Phys.* **86**, 5296 (1999).
14. S. Ishihara, and M. Hanabusa, *J. Appl. Phys.* **84**, 596 (1998).
15. J.Y. Yun, and S.W. Rhee, *Thin Solid Films* **320**, 163 (1998).
16. N. Biunno, J. Narayan, S.K. Homeister, A.R. Srivatsa, and R.K. Singh, *Appl. Phys. Lett.* **54**, 1519 (1989).
17. H. Conrad, *Acta Metall.* **11**, 75 (1963).
18. C. Suryanarayana, *Int. Mater. Review* **40**, 41 (1995).
19. B. Lawn, in *Fracture of Brittle Solids*, 2nd ed. (Cambridge University Press, Cambridge, United Kingdom, 1995), pp. 332–334.
20. H. Conrad and J. Narayan, *Scripta Mater.* **42**, 1025 (2000).
21. J. Narayan, *J. Nanoparticle Res.* **2**, 91 (2000).
22. C.C. Koch and J. Narayan, in *Structure and Mechanical Properties of Nanophase Materials-Theory and Computer Simulation vs Experiment*, edited by D. Farkas, H. Kung, M. Mayo, H. Van Swygenhoven, and J. Weertman (Mater. Res. Soc. Symp. Proc. **634**, Warrendale, PA, 2001), p. B6.1.1.
23. J. Schiotz, F.D. DiTolla, and K.W. Jacobsen, *Nature* **391**, 561 (1998).
24. R. Venkatesan, A.K. Sharma, A. Kvit, Q. Wei, J. Sankar, and J. Narayan, in *Structure and Mechanical Properties of Nanophase Materials-Theory and Computer Simulation vs Experiment*, edited by D. Farkas, H. Kung, M. Mayo, H. Van Swygenhoven, and J. Weertman (Mater. Res. Soc. Symp. Proc. **634**, Warrendale, PA, 2001), p. B5.1.
25. R. Divakar, D. Sundararaman, and S. Ranganathan, *Scripta Met.* **38**, 59 (1998).
26. J. Narayan and J. Washburn, *Phil. Mag.* **26**, 1179 (1972).
27. B.O. Johansson, J-E. Sundgren, J.E. Greene, A. Rockett and S.A. Barnett, *J. Vac. Sci. Technol. A* **3**, 303 (1984).
28. P.B. Mirkarimi, L. Hultman, and S.A. Barnett, *Appl. Phys. Lett.* **57**, 2654 (1990).